

# THE THREE HUNDRED project: Contrasting clusters galaxy density in hydrodynamical and dark matter only simulations

A. Jiménez Muñoz<sup>1</sup>, J.F. Macías-Pérez<sup>\*1</sup>, W. Cui<sup>4</sup>, M. De Petris<sup>3</sup>, A. Ferragamo<sup>3</sup>, and G. Yepes<sup>2</sup>

<sup>1</sup>Univ. Grenoble Alpes, CNRS, Grenoble INP, LPSC-IN2P3, 53, avenue des Martyrs, 38000 Grenoble, France

<sup>2</sup>Departamento de Física Teórica and CIAFF, Módulo 8, Facultad de Ciencias, Universidad Autónoma de Madrid, 28049 Madrid, Spain

<sup>3</sup>Dipartimento di Fisica, Sapienza Università di Roma, Piazzale Aldo Moro, 500185 Roma, Italy

<sup>4</sup>Institute for Astronomy, University of Edinburgh, Edinburgh, UK

## Abstract.

Cluster number count is a major cosmological probe for the next generation of cosmological large scale-structure surveys like the one expected from the Euclid satellite mission. Cosmological constraints will be mainly limited by the understanding of the selection function (SF), which characterize the probability of detecting a cluster of a given mass and redshift. The SF can be estimated by injecting realistic simulated clusters into the survey and re-applying the detection procedure. For this purpose we intend to use THE THREE HUNDREDS project, a 324 cluster sample simulated with full-physics hydrodynamical re-simulations. In this paper we concentrate on the study of the distribution of member galaxies in the cluster sample. First, we study possible resolution effects by comparing low and high resolution simulations. Finally, accounting for the latter we derive the density profiles of the member galaxies and discuss their evolution with cluster mass and redshift.

## 1 Introduction

The next generation of large-scale structure survey instruments, like the Euclid satellite [1] and the Rubin observatory [2], will use cluster abundance as a major cosmological probe to constraint the parameters of the  $\Lambda$ CDM cosmological model. In practice, one needs to compare the total number of observed clusters in a given solid angle region,  $\Omega$ , to the predicted cluster counts as a function of mass and redshift [3]. For this, it is necessary to account for the probability of finding a cluster at a certain mass and redshift in this solid angle, which is known as the Selection Function (SF). The SF is an intrinsic characteristic of the cluster catalogue and depends on the cluster finder algorithm, the observational and quality cuts, and the characteristics of the survey. In order to estimate the SF, it is needed to use simulated data sets. These can be either a full mock galaxy catalogue including clusters and field galaxies, or individual simulated clusters which are injected in the observed galaxy

---

\*e-mail: [macias@lpsc.in2p3.fr](mailto:macias@lpsc.in2p3.fr)

catalogue. Various ways of computing the SF related to different levels of refinement and related to the cluster finder used have been developed [e.g. 3–6].

Large sky volume is needed to find massive objects like galaxy clusters. However, it is difficult to produce simulations including both dark matter and baryons with enough resolution for these large volumes. A solution to this is the ‘zoom’ simulations, as adopted by THE THREE HUNDREDS [7]. For this project, a large cosmological volume is simulated by N-body dark-matter-only simulation, and only in the regions where a galaxy cluster is found, full-physics simulations are performed. For having enough statistics it is necessary to run at least hundreds of independent simulations. We describe in this paper the main optical and IR properties of the THREE HUNDREDS clusters in the prospect of using them for computing the SF of future cluster catalogues like the one expected for the Euclid satellite.

## 2 THE THREE HUNDREDS project

THE THREE HUNDREDS project consists of a 324 cluster sample simulated with full-physics hydrodynamical re-simulations. They have been produced starting from the dark-matter-only MultiDark Simulations [MDPL2 8], which consists in a  $1 h^{-1}$  Gpc cube containing  $3840^3$  dark matter (DM) particles with a mass of  $1.5 \times 10^9 h^{-1} M_{\odot}$  each. The ROCKSTAR halo finder [9] is ran on this simulation to find dark matter haloes. A total of 324 spherical regions were extracted from the halo finder results, selecting as center for these regions the position of the most massive halo at redshift  $z = 0$ . The radius of each spherical region is  $15 h^{-1}$  Mpc that is much larger than the virial radius of the central cluster. The phase space initial conditions for the 324 selected regions are used to perform the ‘zoom’ re-simulations. For the study presented here, THE THREE HUNDREDS collaboration has ran these simulations using the GADGET-X [10] code, which can generate both dark matter only or hydrodynamical simulations. The GADGET-X code[?] is based on a modern version of the Smoothed Particle Hydrodynamics (SPH) first proposed by [11, 12].

Depending on the physics and the resolutions we consider the following THE THREE HUNDREDS simulations in this paper:

1. **LR DMONLY:** Dark-matter-only simulations with a dark matter particle resolution of  $1.5 \times 10^9 h^{-1} M_{\odot}$ . A total of 324 regions have produced.
2. **HR DMONLY:** Dark-matter-only simulations at high resolution. With respect to *LR DMONLY*, it has twice particles per dimension, thus,  $7680^3$ , with eight times less mass per particle i.e.,  $1.8 \times 10^8 h^{-1} M_{\odot}$  each. For these simulations we only have 68 regions. Hence, when comparing with the low resolution simulations with the *HR DMONLY* ones, we will use the 68 regions for which we have high resolution data.
3. **LR HYDRO:** Full-physics hydrodynamics zoom simulations at low resolution. These simulations are at the same resolution as the *LR DMONLY* simulations and 324 regions are available.
4. **HR HYDRO:** Physics as *LR HYDRO* but at high resolution as *HR DMONLY*. Only one region has been simulated because to time constraints. The latter has been mainly used to identify resolution problems, which manifest in the luminosity function of cluster galaxy members.

We concentrate only on the most massive and central cluster of the  $15 h^{-1}$  Mpc region, also called host halo. This is for ensuring large enough clusters that can host a significant

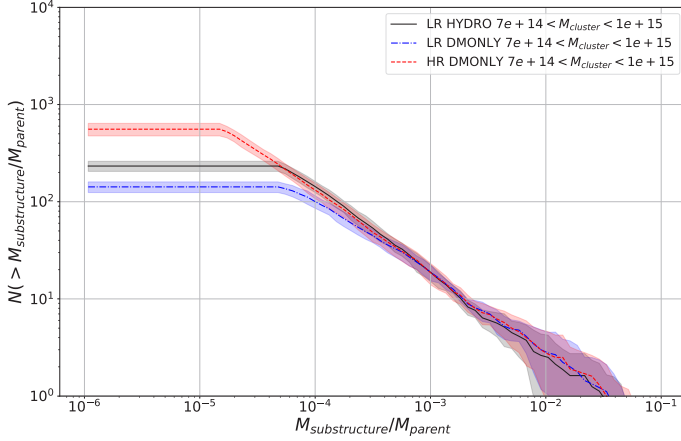


**Figure 1.** 3D cumulative satellite galaxy mass function at  $z = 0$  and  $7 \times 10^{14} M_{\odot} < M < 1 \times 10^{15} M_{\odot}$ . In blue, red and black, for *LR DMONLY*, *HR DMONLY* and *LR HYDRO* simulations, respectively. Each line corresponds to the mean value of 3D galaxy mass functions of the individual clusters in the bin. The shaded regions are the  $1\sigma$  uncertainties coming from the standard deviation across clusters in the mass bins.

number subhalos or substructures, implying a higher galaxy statistics. **A subhalo is defined as a gravitationally bound structure either to the host halo or to another subhalo. The subhalo were identified using a the Amiga’s Halo Finder (AHF) algorithm (see [17]) as discussed in [7]. To define a galaxy, first we consider a mass threshold, for the subhalo mass, for each of three simulations. This translates into a mass resolution limit. Notice that we consider the particle mass instead of the number of particles as our threshold because for the different simulations the particle mass is different. Thus, the same number of particles does not translate into the same subhalo mass. Taking into account the particle mass and the simulation resolution we consider a minimum mass of  $4 \times 10^{10} M_{\odot}$ . In the case of the hydrodynamical simulations, we need also to consider the mass ratio between the dark matter and the star content of the galaxy. We assume that the mass of a real galaxy is mainly coming from the dark matter halo surrounding the stars and gas, so we also impose that the stellar mass component is not higher than 30% of the total mass. For this analysis the galaxies identified within a subhalo will be associated directly to the host halo. In the following, a galaxy will be called substructure or subhalo depending on the context.**

### 3 Subhalo Mass Function

The subhalo mass function, which gives the number of substructures above a given mass relative to the halo mass, can be used to study possible resolution issues. Indeed, the lack of mass resolution in the LR simulation will imprint in this cumulative subhalo mass function as a deficit of low-mass subhalos with respect to the HR ones, as discussed in [13]. In practice, we study this cumulative subhalo mass function defined as the total number of subhalos with relative mass (ratio between their mass and their host halo mass) below a given value. We have divided THE THREE HUNDREDS cluster sample in various bins in mass and redshift. We

selected as narrow bins in mass as possible to ensure that cluster properties within the bin are similar while having a sufficient number of clusters per bin. As an example, we present in Figure 1, the 3D cumulative subhalo mass function at redshift  $z = 0$  for cluster with mass in the range  $7 \times 10^{14} M_{\odot} < M < 1 \times 10^{15} M_{\odot}$ . In the figure, each line corresponds to the mean value of the 3D galaxy mass function of the individual clusters in the bin. The shaded regions are the  $1\sigma$  uncertainties coming from the standard deviation across clusters. For this analysis we consider only the first three simulation sets described in Sect. 2.

For *DMONLY* simulations the main difference is seen for the smaller substructures. We find many more of them from the *HR* simulations. For both mass functions we observe that the cumulative number of structures becomes constant for the smallest masses, indicating that there are no structures smaller than a certain threshold in relative mass ( $M_{\text{sub}}/M_{\text{parent}}$ ). This threshold is different for the *LR* and *HR* simulations. We can see that the three simulations are consistent for the more massive substructures, and again the main differences come from the low-mass subhalos. At the same resolution (i.e., the blue and black lines), we find more objects in the hydro simulation, and these objects are less massive. This could be due to the fact that baryonic physics, such as gas cooling processes, avoid the strip out of the particles in these low-mass subhalos. The slope for the *LR HYDRO* simulations is closer to the *HR DMONLY* but still we can see that the black line is slightly above the red one in the low mass regime. This means that improving the resolution in dark-matter-only simulations is not equivalent to adding baryonic physics in the simulations.

To compare the properties of clusters from the three sets of simulations, we define a relative halo mass ( $M_{\text{sub}}/M_{\text{parent}}$ ) threshold beyond which the resolution effect does not play a significant role. This threshold is defined from the observed plateau in Figure 1 for each set. Note that when comparing the different simulations we will use the highest mass cut for the simulations involved. The mass cut defined from the *DMONLY* and *HYDRO LR* simulations will be called *DMONLY Cut* and *HYDRO Cut* in the following.

## 4 Subhalo Density Distribution

In this section we compare the subhalo density distribution obtained for the different types of simulations discussed above. First of all, we apply the mass cut discussed above to ensure that resolution effects can be neglected. If we use the *LR DMONLY* we will use the *DMONLY Cut* and the *HYDRO Cut* otherwise.

### 4.1 Subhalo density distribution estimation

For each simulation and a given threshold in mass we estimate the subhalo distribution from each cluster in a mass and redshift bin and average it over all the clusters in that bin. Uncertainties are computed from the dispersion across clusters in the same bin. Figure 2 shows the Einasto model fit for the 3D cumulative radial subhalo density profiles for *LR HYDRO* and *HR DMONLY* in black and red respectively, at  $z = 0$  for clusters in the mass range  $7 \times 10^{14} M_{\odot} < M < 1 \times 10^{15} M_{\odot}$ . We observe that the subhalo density distribution of the *LR HYDRO* simulations is overall above the *HR DMONLY* except the cluster outskirts. Note that the decrease of the subhalo density distribution above  $R_{200}$  is just an artifact as no member subhalos are expected beyond this radius for THE THREE HUNDREDS simulations.

To better characterize the difference between the two simulation sets we fit them to an analytical model and check their evolutions with redshift. It has been proven in [14], that for

numerical simulations with an accurate resolution, the Navarro-Frenk-White profile differs from the data, and that the Einasto profile provides a better fit. Thus, we use here the Einasto profile defined by [15, 16] as

$$\rho(r) = n_0 \exp\left(\frac{-2}{\alpha} \left[\left(\frac{r}{r_0}\right)^\alpha - 1\right]\right), \quad (1)$$

where  $n_0$ ,  $r_0$  and  $\alpha$  are the free parameters describing the model. The fit is performed using a MCMC algorithm. We do not use the data beyond  $R_{200}$ , nor radial bins with less than three galaxies (nearby the center of the cluster) for the fit. In practice, we only use the darker regions in the Figure. Note that for the *LR HYDRO* the used region is larger as we have more galaxies in the inner part of the clusters.

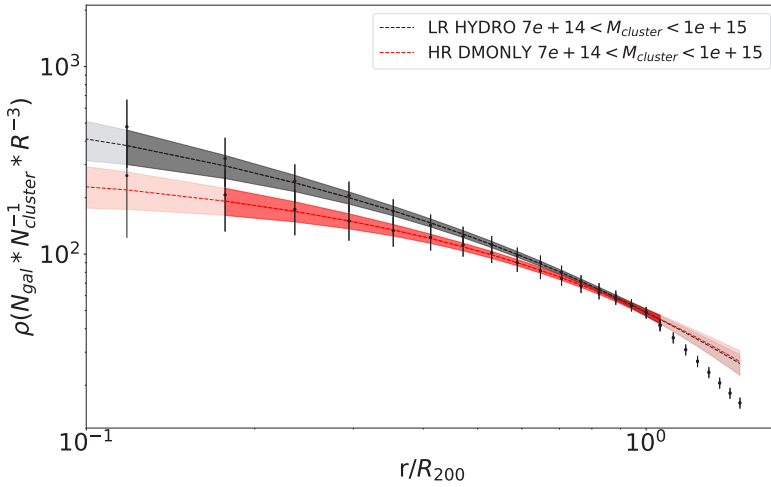


**Figure 2.** Subhalo density radial profiles for the *HR DMONLY* and the *LR HYDRO* simulations when the *HYDRO Cut* is applied, for  $z = 0$  and for cluster mass in the range  $7 \times 10^{14} M_\odot < M < 1 \times 10^{15} M_\odot$ . The dotted lines and the shaded regions correspond to the best-fit Einasto profile with its uncertainties based on the 16th, 50th and 84th percentiles over the posterior distribution of the model parameters.

## 4.2 Evolution in mass and redshift

We repeated the previous process for all mass and redshift bins. Figure 3 shows the 2D posterior probability distribution for parameters corresponding to cluster in the mass range  $7 \times 10^{14} M_\odot < M < 1 \times 10^{15} M_\odot$  for several redshifts between 0 and 1. We show the results by pairs of parameters: 1)  $\alpha$  and  $r_0$ , in the top row, 2)  $r_0$  and  $n_0$ , in the middle row, 3)  $\alpha$  and  $n_0$ , in the bottom row. The shaded colored regions represent the 68 % C.L. uncertainties. In general we observe that  $\alpha$  is lower and  $n_0$  greater for the *LR HYDRO* simulations, and  $r_0$  values are consistent for both types of simulations. A lower value of the slope,  $\alpha$ , and greater of the normalization,  $n_0$ , for a fixed value of  $r_0$  means that the subhalo density profile increases towards the center of the cluster and drops rapidly in the outskirts. This consistent with the difference between *LR HYDRO* and *HR DMONLY* simulations observed in Figure 2. At high redshift this behaviour is accentuated as  $\alpha$  decreases with redshift, while  $n_0$  increases. The fact that  $n_0$  increases with redshift can be due to that at high redshift there is more fragmentation, and then a larger number of galaxies is giving a higher density value.

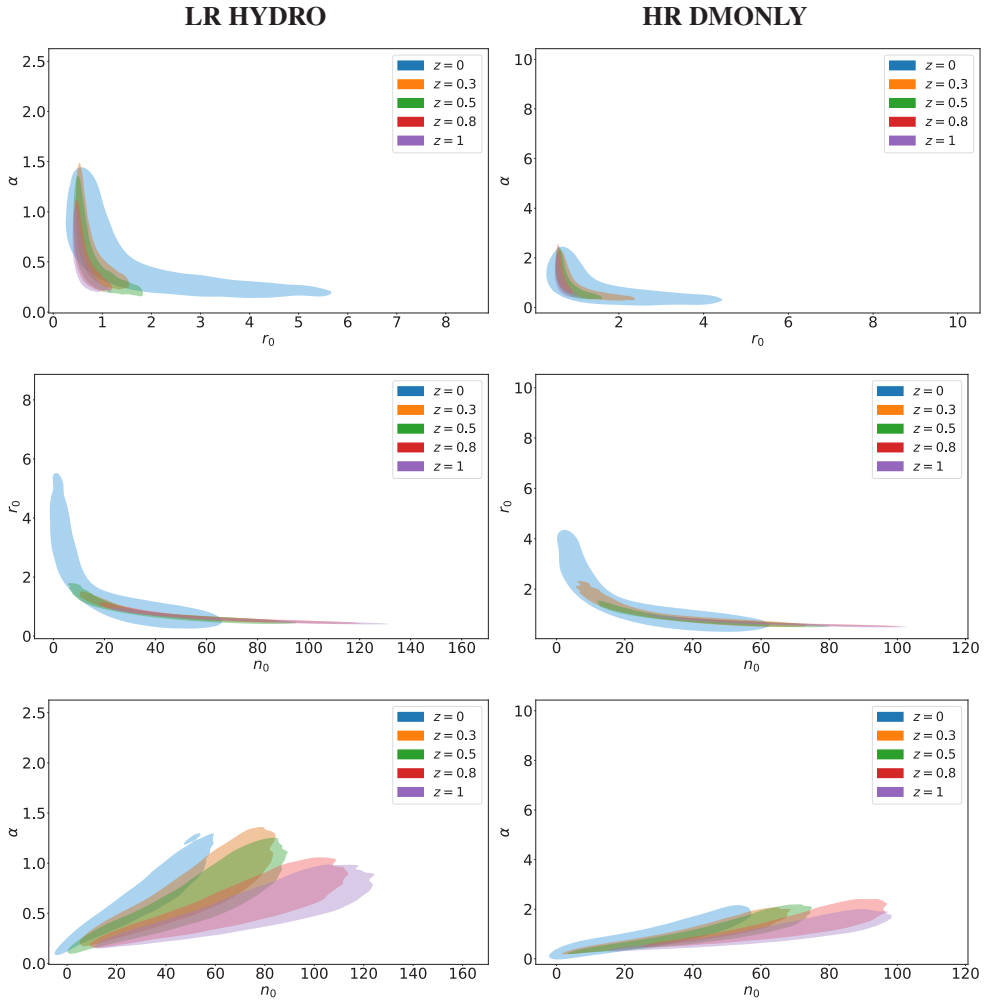


**Figure 3.** Evolution with redshift of 2D probability distributions for the  $n_0$ ,  $\alpha$  and  $r_0$  parameters of the Einasto model. In the left and right columns we show the *LR HYDRO* and *HR DMONLY* simulations, respectively. The shaded regions correspond to the 68 % C.L.

## 5 Conclusions

The determination of the cluster selection function will be crucial to perform cluster cosmology with the next generation of large-scale structure experiments as the Euclid satellite and the Rubin observatory. To compute the SF, large simulations with realistic cluster properties are needed. At this respect, we have investigated here the properties of the clusters of THE THREE HUNDRED PROJECT. For this we consider low and high resolution dark-matter-only and hydrodynamical simulations.

We have identified a resolution effect in THE THREE HUNDREDS low resolution simulations, which does not allow us to study the luminosity function. These effects were identified previously by [13] but with a much lower statistics and much sparse coverage in mass and redshift.

Studying the density mass function for the different sets of simulations we have been able to set subhalo mass thresholds above which resolution effects are negligible for the determination of the subhalo density distribution.

Using a common cut we have determined and compared the subhalo density distribution for the *DMONLY* and *HYDRO* simulations. We find that the latter preserve more structures and in particular towards the center of the cluster. This difference increases with redshift. We have also found that the Einasto profile is a good fit to the density of subhalos.

## References

- [1] Laureijs et al., arXiv:1110.3193 (2011).
- [2] Abell et al., arXiv:0912.0201 (2009).
- [3] Sartoris et al., Monthly Notices of the Royal Astronomical Society, **459**, 1764-1780 (2016)
- [4] Maturi et al., Monthly Notices of the Royal Astronomical Society, **485**, 498-512 (2019)
- [5] Adam et al., Astronomy & Astrophysics, **122**, 399-407 (2019)
- [6] Rykoff et al., The Astrophysical Journal, **785**, 104 (2014)
- [7] Cui et al., Monthly Notices of the Royal Astronomical Society **480**, 2898–2915 (2018).
- [8] Giocoli et al., Monthly Notices of the Royal Astronomical Society **461**, 209-223 (2016)
- [9] Behroozi et al., The Astrophysical Journal, **762**, 109 (2013)
- [10] Beck et al., Monthly Notices of the Royal Astronomical Society, **455**, 2110-2130 (2016)
- [11] Lucy, L.B., The astronomical journal, **82**, 1013-1024 (1977)
- [12] Gingold et al., Monthly notices of the royal astronomical society, **181**, 375-389 (1977)
- [13] Dolag et al., Monthly Notices of the Royal Astronomical Society, **399**, 497-514 (2009)
- [14] Navarro et al., Monthly Notices of the Royal Astronomical Society, **402**, 21-34 (2010)
- [15] Einasto et al., Trudy Astrofizicheskogo Instituta Alma-Ata, **5**, 87-100 (1965)
- [16] Navarro et al., Monthly Notices of the Royal Astronomical Society, **349**, 1039-1051 (2004)
- [17] Knollmann & Knebe, the Astrophysical Journal Supplement, **182**, 608-624 (2009)